nature materials

ARTICLES

PUBLISHED ONLINE: 19 JUNE 2011 | DOI: 10.1038/NMAT3049

Nanoparticles that communicate *in vivo* to amplify tumour targeting

Geoffrey von Maltzahn[1,2], Ji-Ho Park[3], Kevin Y. Lin[4], Neetu Singh[1], Christian Schwöppe[5], Rolf Mesters[5], Wolfgang E. Berdel[5], Erkki Ruoslahti[6,7], Michael J. Sailor[8,9] and Sangeeta N. Bhatia[1,10,11,12]★

Nanomedicines have enormous potential to improve the precision of cancer therapy, yet our ability to efficiently home these materials to regions of disease *in vivo* remains very limited. Inspired by the ability of communication to improve targeting in biological systems, such as inflammatory-cell recruitment to sites of disease, we construct systems where synthetic biological and nanotechnological components communicate to amplify disease targeting *in vivo*. These systems are composed of 'signalling' modules (nanoparticles or engineered proteins) that target tumours and then locally activate the coagulation cascade to broadcast tumour location to clot-targeted 'receiving' nanoparticles in circulation that carry a diagnostic or therapeutic cargo, thereby amplifying their delivery. We show that communicating nanoparticle systems can be composed of multiple types of signalling and receiving modules, can transmit information through multiple molecular pathways in coagulation, can operate autonomously and can target over 40 times higher doses of chemotherapeutics to tumours than non-communicating controls.

Advances in nanotechnology have produced a diverse toolkit of individual nanodevices with unique electromagnetic properties[1–3] and the ability to encapsulate and programmably release a diversity of therapeutics[4–9], yet the ultimate biomedical efficacy of such devices largely depends on their *in vivo* fate. Over the past three decades, approaches to targeting nanomaterials *in vivo* have focused on tuning the properties of individual nanoparticles (NPs) including geometry, surface chemistry, ligand type and ligand density[10–18]. These materials are typically administered as populations of >1 trillion NPs to carry out identical, competitive functions *in vivo*. Here, inspired by the power of communication to improve targeting across multiple length scales in biological systems (for example, insect swarming, immune-cell trafficking, platelet self-assembly), we considered the design of NP systems that communicate to enhance *in vivo* diagnostics, regenerative medicines and therapeutics.

We set out to construct two-component nanosystems from well-characterized NP and biological components, wherein signalling modules would first target tumours and then broadcast the tumour's location to receiving NPs in circulation (Fig. 1a). To facilitate rapid and robust signal transmission in regions of tumour growth, we sought to harness the machinery of an endogenous multistep biological cascade to transmit communications (Fig. 1b) and selected the coagulation cascade due to its powerful signal amplification, positive feedback, ubiquitous presence in plasma and potential to operate across multiple tumour types (Fig. 1c). We hypothesized that two signalling modules could selectively activate the coagulation cascade in tumours: NPs (gold nanorods, NRs) that target tumours and convert external electromagnetic energy into heat to locally disrupt tumour vessels, and engineered human proteins (tumour-targeted tissue factor, tTF) that autonomously survey host vessels for angiogenic tumour receptors and, in their presence, activate the extrinsic coagulation pathway (Fig. 1c).

Receiving modules were constructed using two nanomaterial platforms: a prototypical imaging agent (magnetofluorescent iron oxide nanoworms, NWs) and a prototypical therapeutic agent (doxorubicin-loaded liposomes, LPs). We explored the potential to route communication to receivers through two molecular pathways in coagulation by developing peptide coatings that recognize fibrin directly and peptides that target coagulation enzyme activity by acting as a substrate for the coagulation transglutaminase factor XIII (FXIII) (Fig. 1c).

We first set out to examine the capacity of signalling modules to precisely induce coagulation in tumours (Fig. 2a). To test our hypothesis that photothermal heating of gold NRs could disrupt tumour blood vessels to initiate extravascular coagulation[19–22], we examined the transduction of tumour heating into localized coagulation by evaluating fibrin deposition in tumours as a function

[1]Harvard–MIT Division of Health Sciences and Technology, Massachusetts Institute of Technology, 77 Massachusetts Avenue, Cambridge, Massachusetts 02139, USA, [2]Flagship VentureLabs, Flagship Ventures, 1 Memorial Dr. 7th Fl, Cambridge, Massachusetts 02142, USA, [3]Department of Bio and Brain Engineering, Korea Advanced Institute of Science and Technology, 291 Daehak-ro, Yuseong-gu, Daejeon 305-701, South Korea, [4]Department of Chemical Engineering, Massachusetts Institute of Technology, 77 Massachusetts Avenue, Cambridge, Massachusetts 02139, USA, [5]Department of Medicine/Hematology and Oncology, University Hospital Muenster, D-48129 Muenster, Germany, [6]Vascular Mapping Laboratory, Center for Nanomedicine, Sanford-Burnham Medical Research Institute at UCSB, 3119 Biology II Bldg, University of California, Santa Barbara, California 93106-9610, USA, [7]Cancer Research Center, Sanford-Burnham Medical Research Institute, La Jolla, California 92037, USA, [8]Materials Science and Engineering Program, Department of Chemistry and Biochemistry, University of California, San Diego, 9500 Gilman, La Jolla, California 92093, USA, [9]Department of Chemistry and Biochemistry, University of California, San Diego, La Jolla, California 92093-0358, USA, [10]Electrical Engineering and Computer Science, MIT, Massachusetts 02142, USA, [11]David H. Koch Institute for Integrative Cancer Research, MIT, Massachusetts 02142, USA, [12]Department of Medicine, Brigham and Women's Hospital, Howard Hughes Medical Institute, Massachusetts 02115, USA. *e-mail: sbhatia@mit.edu.

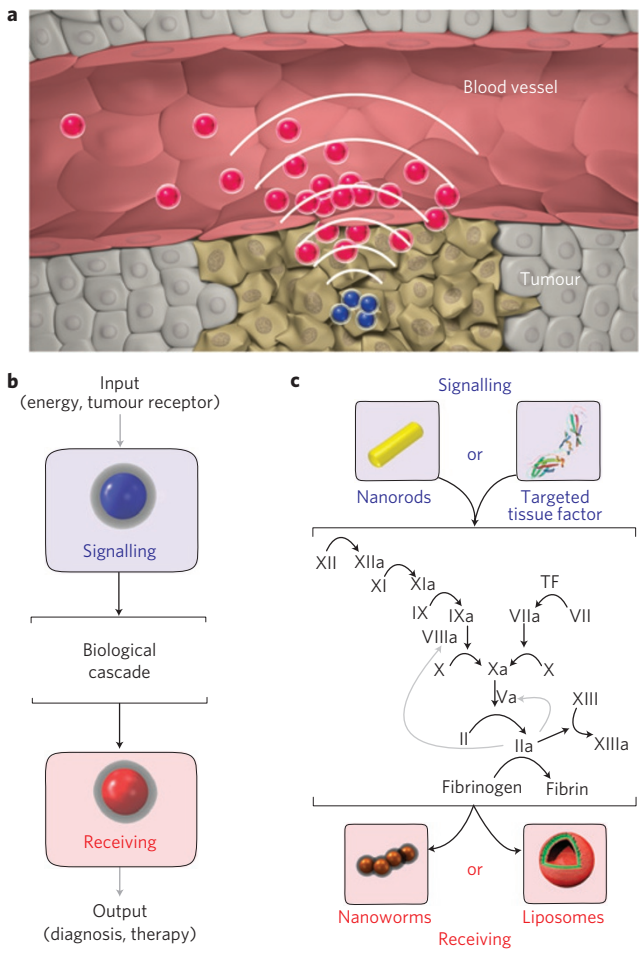

Figure 1 | Nanoparticles communication for amplified tumour targeting. **a**, Schematic representation of communication between system components. Tumour-targeted signalling NPs broadcast the tumour location to receiving NPs in circulation. **b**, Harnessing a biological cascade to transmit and amplify NP communications. **c**, Molecular signalling pathway between the signalling and receiving components. Signalling and receiving components act as unnatural inputs and outputs to the coagulation cascade, respectively. Signalling components are either tumour-targeted plasmonic gold NRs, which initiate coagulation cascade activation in tumours by photothermally disrupting tumour vessels and activating the extrinsic and intrinsic coagulation pathways, or tumour-targeted truncated tissue factor proteins, which are latent in circulation and activate the extrinsic coagulation pathway on binding to tumour receptors. Communication is exploited to recruit inorganic (iron oxide nanoworms) or organic (drug-loaded LPs) receiving components through activity of the coagulation transglutaminase FXIII or through targeting of polymerized fibrin.

of temperature (Fig. 2a). Purified fibrinogen (the precursor to fibrin) and albumin (an abundant blood protein unrelated to coagulation) were labelled with unique near-infrared (NIR) fluorochromes to allow simultaneous assessment of coagulation-dependent and independent protein tropism to heated tumours. Mixtures of fibrinogen and albumin were intravenously injected into athymic (*nu/nu*) mice bearing bilateral human MDA-MB-435 tumours, after which one tumour was heated using a temperature-controlled water bath. At 24 h, mice were killed and the relative levels of tumour fibrin(ogen) and albumin were assessed fluorescently. We observed a marked induction of fibrin(ogen) accumulation in tumours between 45 °C and 53 °C, with little accompanying increase in albumin accumulation, indicating that heat specifically directed coagulation-cascade activation in tumours (Fig. 2b, Supplementary Fig. S1). Immunohistochemical staining for fibrin(ogen) in tumours from uninjected mice corroborated these findings, demonstrating that exogenous fibrinogen administration did not artificially drive accumulation in heated tumours (Supplementary Fig. S1).

Having probed the thermal sensitivity of coagulation in tumours, we next investigated whether tumour-targeted gold NRs could specify coagulation to occur in tumour tissues. Rod-shaped gold NPs are precisely tunable plasmonic nanomaterials that may be synthesized in bulk, have narrow size distributions and have optical absorption coefficients 10^4–10^6 times higher than those of conventional organic fluorochromes[19–21]. Previously, we demonstrated that polyethylene glycol-coated gold NRs (PEG–NRs) have >17 h circulation half-lives in mice and can passively target tumours in mice through their fenestrated angiogenic blood vessels to direct precise tumour heating with otherwise benign NIR energy (Supplementary Fig. S2; refs 23–25). Because NIR light can penetrate several centimetres in human tissue, it provides an attractive external input to actuate vascular disruption in tumours[26]. To examine NR-directed coagulation, PEG–NRs (10 mg Au kg^{-1}) or saline were intravenously administered to mice bearing bilateral MDA-MB-435 tumours (Fig. 2c,d). After PEG–NR clearance from circulation (72 h post-injection), fluorescent fibrinogen was intravenously injected and the right flanks of mice were irradiated with NIR light (~1 W cm^{-2}), generating focal tumour surface temperatures of ~49 °C in PEG–NR-injected mice, while saline-injected tumour surface temperatures remained below ~37 °C (Fig. 2c). At 24 h post-injection, irradiated tumours on NR-injected mice displayed localized accumulation of fibrinogen (Fig. 2d), while tumours with PEG–NRs or NIR energy alone and peripheral tissues lacked this feature. Histopathological analysis revealed that fibrin(ogen) deposition formed a broad interstitial mesh in heated tumours, indicating that NR heating could disrupt tumour blood vessels to activate extravascular coagulation (Supplementary Fig. S2).

We next investigated the potential for a biological signalling module to autonomously survey the host vasculature for angiogenic tumour receptors and, in their presence, engage the extrinsic coagulation cascade. Such a system would operate without the need for any external electromagnetic inputs (for example NIR energy) and could potentially amplify NP targeting to deep-seated and disseminated cancers. We used a truncated, tumour-targeted version of the human protein tissue factor (tTF–RGD), which harnesses an RGD peptide motif to induce coagulation on binding to angiogenic $\alpha_v\beta_3$ receptors[27–31] (Fig. 2e). When tTF is separated from essential cell surface lipid co-factors, its activity towards FX activation diminishes by five orders of magnitude[32]. This nearly digital dependence on cell-surface localization has enabled tumour-targeted tTFs to specifically activate coagulation in mouse cancer models and, recently, in human cancer patients[27,28]. As with PEG–NR signalling modules, we first probed the relative accumulation of fluorescently labelled fibrinogen and albumin in MDA-MB-435 tumours of mice injected with varying doses of tTF–RGD proteins. At 24 h after injection, we observed a macroscopic appearance of haemorrhage in tumours on mice injected with tTF–RGD (>15 μg tTF–RGD/mouse), corresponding to the tumour-specific accumulation of fibrinogen in dendritic, vascular patterns, which were absent from control tumours (Fig. 2f,g, Supplementary Fig. S3). Microscopically, this appearance of vascular coagulation was corroborated by the abundant localization of fibrin(ogen) within tumour blood vessels (Fig. 2g).

Together, we found that both PEG–NR and tTF–RGD signalling modules produced tumour-specific coagulation, highlighting the potential for localized coagulation to communicate the tumour's location to receivers in circulation. We next set out to develop receiving NPs that could efficiently target regions of coagulation

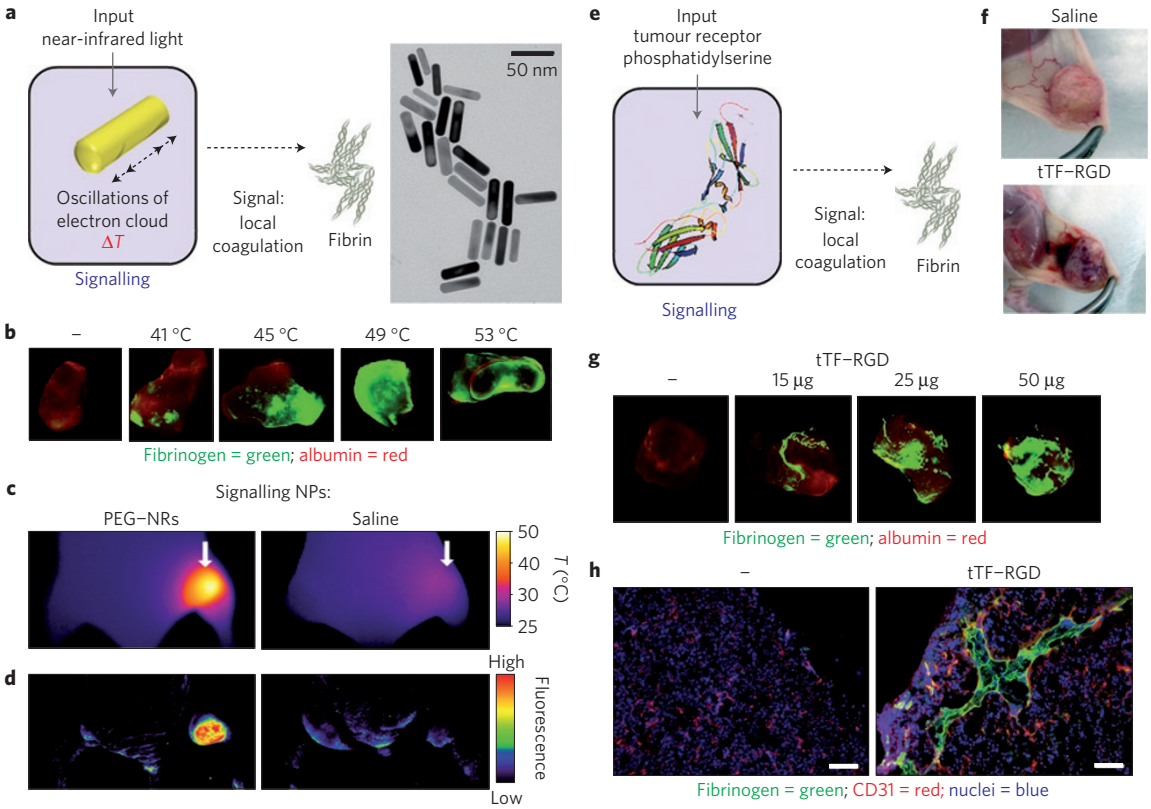

Figure 2 | 'Signalling' component characterization. a, Schematic representation of NR-directed coagulation and transmission electron microscopy of NIR-absorbing NRs. Gold NRs are targeted to tumours to specify local coagulation-cascade activation through photothermal conversion of NIR energy. **b**, Probing the coagulation-dependent and independent protein tropism to heated tumours. Fibrinogen and albumin were labelled with unique NIR fluorochromes and injected into mice bearing bilateral MDA-MB-435 tumours. Immediately following injection, one tumour on each mouse was heated using a temperature-controlled water bath. At 24 h post-injection, mice were dissected and tumours imaged for the relative abundance of fibrinogen (green) and albumin (red). **c**, Thermographic imaging of PEG-NR- and saline-injected mice under NIR irradiation of the right flank. **d**, Fluorescence reflectance imaging of mice to visualize fibrinogen tropism to PEG-NR-heated tumours. **e**, Schematic representation of tumour-targeted tissue factor stimulation of the coagulation cascade in response to tumour receptors. Signalling components are ligand-targeted, truncated human tissue factor proteins (tTF-RGD) proteins that are latent in circulation and autonomously gain coagulation-inducing activity on binding to $\alpha_v\beta_3$ receptors in tumour blood vessels and associating with endothelial cell surface phosphatidylserine. **f**, Intraoperative images at 24 h post tissue factor injection revealing tTF-RGD-mediated haemorrhaging. **g**, Probing the coagulation-dependent and independent protein tropism to tumours on tTF-RGD-injected mice. tTF-RGD signalling components were injected intravenously at varying doses alongside mixtures of fluorescent fibrinogen (green, VT750) and albumin (red, VT680) to monitor tTF-RGD-mediated coagulation in tumours. **h**, Histopathologic analysis of tumour fibrinogen distribution without (left) and with (right) 25 μg tTF-RGD signalling component co-injection (red = CD31 blood-vessel stain; green = injected fibrinogen fluorescence; blue = nuclear stain; scale bars = 100 μm).

to deliver therapeutics or act as imaging agents (Fig. 3a). Initially, magnetofluorescent iron oxide nanoworm imaging agents (NWs; Fig. 3b top) were derivatized with a peptide substrate for the coagulation transglutaminase FXIII (G–N– **Q**–E–Q–V–S–P–L–T–L–L–K–X–C–fluorescein)[33–35] to enable receiver incorporation into regions of active coagulation (Fig. 3b bottom, Supplementary Fig. S4). Having observed that external heating of tumours produced localized coagulation, we used this response in an assay to assess the ability of receivers to target tumour coagulation before integrating them with signalling modules. Mixtures of targeted and untargeted NWs, labelled with unique NIR fluorochromes, were intravenously injected into mice bearing two MDA-MB-435 tumours. Immediately following injection, one tumour was submerged in a temperature-controlled water bath for 20 min and mice were dissected at 24 h for fluorescent organ imaging. We found that the accumulation of FXIII–NW receivers was sharply amplified at 45 °C compared with FXIIIControl–NW-bearing peptides without the essential glutamine for FXIII cross-linking (Fig. 3c,d, Supplementary Fig. S5), enabling nearly an order-of-magnitude increase in tumour targeting compared with unheated tumours. The specificity of heat-induced targeting to coagulation persisted up to 53 °C, although the magnitude of accumulation decreased (Fig. 3e), probably indicating that higher temperatures accelerated intravascular coagulation and occlusion, diminishing the perfusion required for delivery of receiving NWs into tumours. Histopathologically, FXIII–NWs showed marked extravasation and interstitial spreading in heated tumours compared with controls (Fig. 3d, Supplementary Fig. S5), illustrating the capacity of thermal energy to dismantle tumour vascular barriers and direct abundant interstitial receiver accumulation.

We also explored the feasibility of channelling communications through an alternative molecular pathway in the coagulation cascade. NWs were derivatized with a fibrin-binding peptide (Ac–d–d–d–**G–Y–e–C–hyP–cY–G–L–C–Y–I–Q**–K–fluorescein; Fig. 3b) and tested in a similar assay. Fibrin-binding receiving NWs also exhibited nearly a tenfold amplification of targeting to heated tumours (Fig. 3c, Supplementary Fig. S5), with prominent extravascular accumulation histopathologically (Supplementary Fig. S5).

We next constructed model therapeutic receiving modules to provide amplified drug delivery to regions of tumour

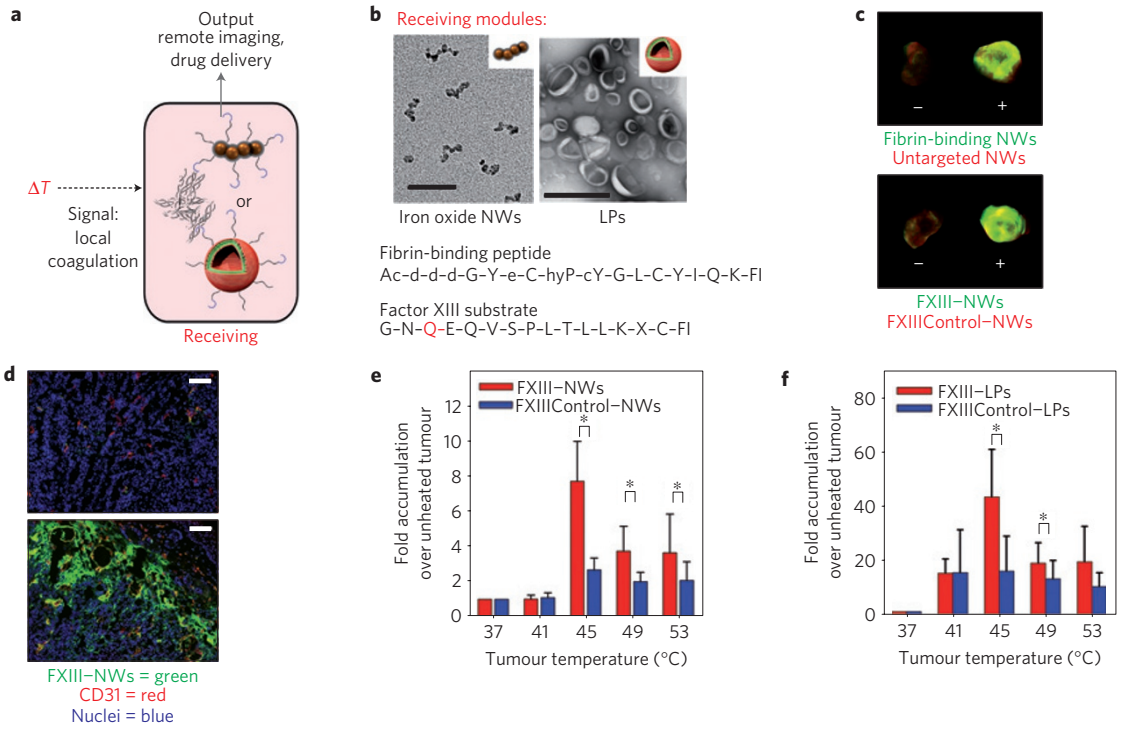

Figure 3 | 'Receiving'-component synthesis and testing. a, Schematic representation of receiving-NP homing to regions of coagulation. NW imaging agents and drug-loaded LPs (top and bottom, respectively) were derivatized with coagulation-targeting peptides to form receiving NPs. **b**, Nanostructure and targeting ligands of receiving NPs. Transmission electron microscopy images of the two classes of nanomaterials used in receiving-NP synthesis: iron oxide NWs (scale bar = 50 nm) and doxorubicin-loaded LPs (scale bar = 400 nm). Two peptides were used to generate receiving NPs: a fibrin-binding peptide and a glutamine-containing substrate for the coagulation transglutaminase FXIII to respectively direct particle binding and covalent attachment in regions of coagulation. **c**, Fluorescence reflectance imaging of receiving-NP homing to externally heated tumours. Mixtures of targeted (green) and untargeted (red) NWs, labelled with the unique NIR fluorochromes VT750 and VT680, respectively, were intravenously injected into mice bearing bilateral MDA-MB-435 tumours. Immediately following injection, one tumour was submerged in a temperature-controlled water bath for 20 min and mice were dissected at 24 h for fluorescent organ imaging. Overlaid fluorescence images are shown for targeted (green) and untargeted (red) receiving-NP accumulation in both heated (+, 45 °C heating) and naive (−) tumours from the same mouse. **d**, Histopathological analysis of receiving-NP homing to heated tumours. Histological sections from naive (top) and heated (bottom, 45 °C) tumours in FXIII-NW-injected mice were stained for CD31 (red) and nuclei (blue) and imaged to reveal receiving-NP distribution (green). (Scale bars = 100 μm.) **e**, Quantifying the amplification of FXIII-NW and FXIIIControl-NW receiver homing to heated over unheated tumours. The fold enhancement of NW targeting is plotted across the range of temperatures tested ($P = 0.02$, 0.03 and 0.04 for the difference between FXIII-NWs and FXIIIControl-NWs at 45 °C, 49 °C and 53 °C, respectively; paired, two-sided t-test, $n = 4$; error bars = s.d.). **f**, Quantifying the amplification of FXIII-LP and FXIIIControl-LP receiver homing to heated over unheated tumours. The fold enhancement of doxorubicin accumulation in tumours is plotted across the range of temperatures tested for FXIII-LPs and FXIIIControl-LPs ($P = 0.025$ and $P = 0.049$ for the difference between FXIII-NWs and FXIIIControl-NWs at 45 °C and 49 °C, respectively; unpaired, two-sided t-test, $n = 3$; error bars = s.d.).

coagulation. Therapeutic receivers were developed by synthesizing doxorubicin-loaded LPs with tethered active (FXIII) or inactive (FXIIIControl) substrates (Supplementary Figs S4, S6). Here, tumour heating to 45 °C directed the accumulation of over 40 times higher doses of doxorubicin in tumours compared with unheated controls and significantly enhanced targeting over inactive FXIIIControl substrate-modified LPs (Fig. 3f).

Having developed signalling and receiving modules and characterized their functions in isolation, we proceeded to study the ability of integrated NP systems to communicate and amplify tumour targeting *in vivo* (Fig. 4a). We began by testing the ability for communication to amplify the targeting of magnetofluorescent FXIII–NW receiving modules to tumours. PEG–NRs (or saline) were intravenously injected into mice bearing bilateral MDA-MB-435 tumours. After NR clearance from circulation (72 h), mixtures of active and inactive receiving NPs (FXIII–NWs and FXIIIControl–NWs) labelled with distinct NIR fluorochromes were co-injected intravenously, followed by NIR irradiation of the entire right flank of the mouse (~0.75 W cm^{-2}, 810 nm, 20 min) under infrared thermographic observation. At 96 h, the entire mouse and then the individual explanted organs were fluorescently imaged (Fig. 4b). Thermographic surveillance of photothermal heating showed focal tumour heating only in NR-injected mice (Fig. 4c) and whole-animal imaging at 96 h revealed pronounced homing of FXIII–NWs to NR-heated tumours, with over an order-of-magnitude increase in accumulation above unirradiated contralateral tumours and tumours on saline-injected mice (Fig. 4d,e, Supplementary Fig. S7). Histologically, integrated NP systems produced intense regions of FXIII–NW fluorescence relative to controls, particularly in tumour boundaries where blood vessels were well perfused (Supplementary Fig. S8). NP systems were found to be effective in xenograft cervical tumour models as well, directing several-fold amplification in homing of targeted receiving NPs over untargeted controls (Supplementary Fig. S9).

We next probed the ability of autonomous communication between tTF–RGD signalling modules and FXIII–NW receiving modules to amplify tumour targeting (Fig. 4f). When co-injected alongside FXIII–NW receivers (Fig. 4g), we find that tTF–RGD signalling modules amplify receiver targeting by several-fold over non-communicating controls and over NWs that are

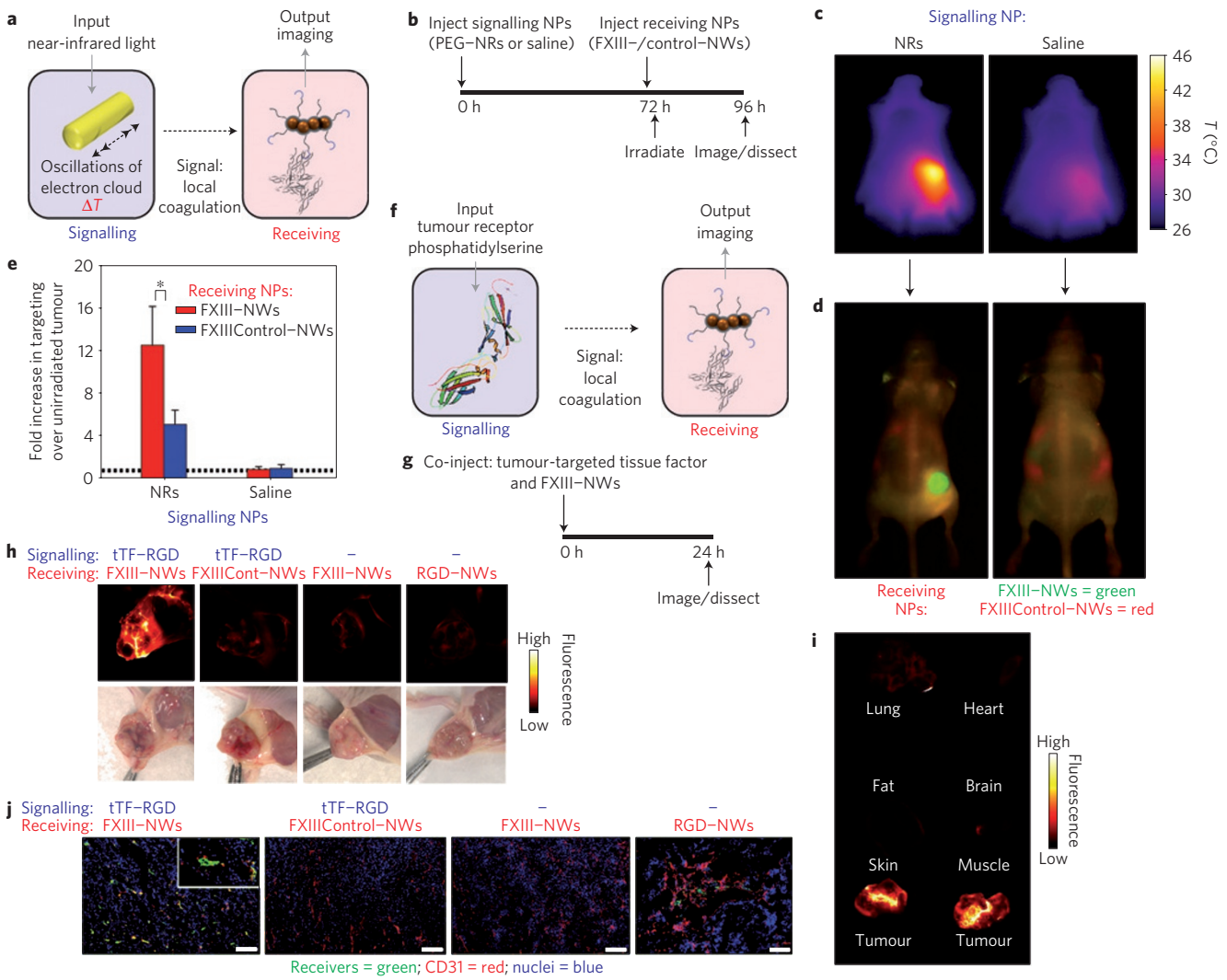

Figure 4 | Amplified tumour targeting with two systems of communicating NPs. a, Schematic representation of communicating NPs. **b**, Experimental timeline for testing communicating NPs. **c**, Thermographic imaging of photothermal PEG–NR heating. At 72 h post NR or saline injection (10 mg Au kg^{-1}), mice were co-injected with coagulation-targeted FXIII–NWs and untargeted FXIIIControl–NWs and their right flanks were broadly irradiated (810 nm, ~0.75 W cm^{-2}, 20 min) under infrared thermographic surveillance to reveal surface temperatures. **d**, Overlaid fluorescence reflectance image of targeted and untargeted receiving-NP homing. At 24 h post-irradiation, whole-animal fluorescence imaging revealed the distributions of coagulation-targeted (FXIII–NWs, green) and untargeted (FXIIIControl–NWs, red) receiving NPs. **e**, Quantification of receiving-NP homing in irradiated versus contralateral unirradiated tumours. After whole-animal imaging, mice were dissected and the fluorescence of each tumour was measured to quantify the homing of receiving NPs. (∗ indicates $P = 0.02$, paired, two-sided t-test; $n = 4$; error bars = s.d.) **f**, Schematic representation of a nanosystem that communicates autonomously in the presence of tumour receptors. **g**, Experimental timeline for testing the autonomous nanosystem *in vivo*. **h**, Intraoperative imaging of NW receivers. *Nu/nu* mice bearing a single MDA-MB-435 tumour were intravenously injected with communicating (tTF–RGD + FXIII–NWs) or control (tTF–RGD + FXIIIControl–NWs) systems, FXIII–NWs alone or NWs targeted by the peptide used to direct signalling-component tumour homing (1 mg kg^{-1} tTF–RGD). At 24 h post-injection, tumours were surgically exposed for fluorescent intraoperative imaging of NW homing. (FXIIICont–NWs = FXIIIControl–NWs.) **i**, Tumour specificity of the autonomous nanosystem. Excised organs from mice injected with autonomously communicating nanosystems (tTF–RGD + FXIII–NWs) were imaged for NW fluorescence at 24 h post-injection (1 mg kg^{-1} tTF–RGD). **j**, Histopathological analysis of NW receivers. Histopathological sections from experiments in **h**. At 24 h post-NW injection, mice were killed and tumours were analysed for NW receiver distribution in histology. (Red = CD31 blood-vessel stain, blue = 4,6-diamidino-2-phenylindole nuclear stain, green = NW receiver distribution, RGD–NW scale bar = 100 μm; all others = 200 μm.)

directly targeted by RGD-targeting ligands (Fig. 4h, Supplementary Fig. S10). Similar to the fibrin(ogen) distribution observed during tTF–RGD signalling-module testing, FXIII–NW receivers injected alongside tTF–RGD proteins produced a dendritic pattern of accumulation in tumours, corresponding to abundant intravascular localization immunohistochemically (Fig. 4h–j). This amplified vascular targeting was found to be specific for tumours over normal organs and was absent when the coagulation inhibitor heparin was administered alongside signalling and receiving modules (Fig. 4i, Supplementary Fig. S10). Further, we found that tTF–NGR signalling modules, which target CD13 angiogenic receptors, were also able to amplify receiver targeting to tumours (Supplementary Fig. S10), highlighting the capacity for autonomously communicating systems to be customized for specific molecular cancer signatures.

As a proof of principle that NP communication could improve tumour drug delivery and therapy, we studied the efficacy of a therapeutic communicating nanosystem (Fig. 5a). We found that

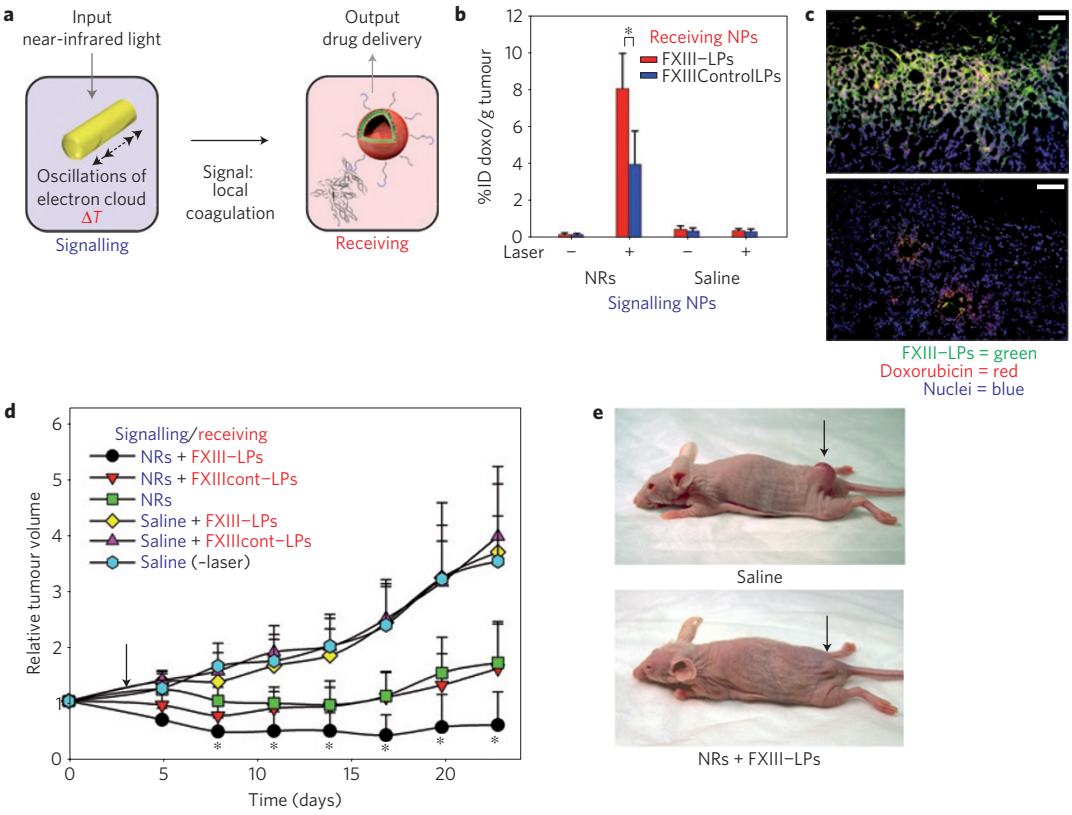

Figure 5 | Amplified tumour therapy with communicating NPs. a, Schematic representation of a therapeutic system of communicating NPs. **b**, Quantification of doxorubicin-loaded LP receiver homing in irradiated versus contralateral unirradiated tumours. At 96 h after signalling NP injection, mice were dissected and the doxorubicin fluorescence of each tumour homogenate in acidic ethanol was measured to quantify the homing of receiving NPs. (∗ indicates $P = 0.021$, unpaired, two-sided t-test, $n = 4$; error bars = s.d.). **c**, Histopathological analysis of NR-directed FXIII-LP targeting and doxorubicin delivery. Histopathological sections from the integrated NP signalling experiments in **b**. At 24 h post NW injection, mice were killed and tumours were analysed for FXIII-LP and doxorubicin distributions in histology. (Red = doxorubicin, blue = 4, 6-diamidino-2-phenylindole nuclear stain, green = FXIII-LP distribution.) (Scale bars = 100 μm.) **d**, Tumour volumes following a single treatment with communicating NP systems and controls. Tumours in all treatment groups except 'Saline (− laser)' were exposed to NIR irradiation for 20 min (~0.75 W cm^{-2}, ~810 nm, arrow) 72 h after intravenous NR or saline injection ($P < 0.05$ for NR + FXIII-LPs and all other treatment sets between days 8 and 24; analysis of variance, $n = 7$ mice in each set; error bars = s.d.). **e**, Representative images of mice treated with communicating NPs (NRs + FXIII-LPs, below) compared with untreated controls (Saline, above) (20 d post-treatment).

communication between NR signalling modules and FXIII–LP receivers amplified the accumulation of doxorubicin in tumours by over 40-fold (~8% ID g^{-1}) as compared with the LPs alone (Fig. 5b) and more than sixfold when compared with an optimized LP formulation that targeted endogenous vascular receptors ($\alpha_v\beta_3$ for high-affinity cyclic-RGD peptide-targeted LPs), illustrating the potential for NP communication to amplify drug delivery over NPs directly targeted to tumour receptors (Supplementary Fig. S11). This amplification of drug delivery probably has at least two components: heat-dependent increases in passive accumulation due to improved extravasation in tumours (as indicated by FXIIIControl–LPs and consistent with previous observations[22]) and specific biochemical recognition of the coagulation process by the peptide coating. Histologically, FXIII–LPs formed a broad interstitial mesh in NR-heated tumours, with released doxorubicin fluorescence emanating from the nuclei of surrounded tumour cells, confirming the delivery and release of active drug within tumour tissues (Fig. 5c).

We finally evaluated the therapeutic efficacy of communicating NPs in mice bearing single MDA-MB-435 human carcinoma tumours. PEG–NRs (10 mg kg^{-1}) or saline were injected into mice and, once NRs had cleared from circulation (72 h), a single intravenous dose of FXIII–LPs, FXIIIControl–LPs or saline (2 mg kg^{-1} doxorubicin) was given, followed immediately by irradiation with NIR energy (~0.75 W cm^{-2}, 810 nm, 20 min). We found that a single treatment with communicating NPs directed a prolonged inhibition of tumour growth that was significantly more effective than system components in isolation (FXIII–LPs, FXIIIControl–LPs, NRs) and non-communicating control systems (NRs + FXIIIControl–LPs; Fig. 5d,e; $p < 0.05$ for NR + FXIII–LPs compared with all other treatment groups at each day from 5 to 24 after treatment; one-sided t-test) without detectable weight loss due to systemic toxicity (Supplementary Fig. S11).

Inspired by communication in biological systems, we devised NP systems that communicate to amplify tumour targeting. We demonstrated that systems of synthetic human proteins and simple NPs can be engineered to transmit information through endogenous biological pathways by acting as artificial inputs and outputs to the coagulation cascade. In contrast with 'combination' therapies, where multiple disease pathways in the host are targeted simultaneously, our strategy was composed of components that communicate with one another to more efficiently target regions of disease. We found that communication through the coagulation cascade enhanced the accumulation of receiving modules in tumours by up to 40-fold relative to receiving modules tested in the absence of communication (Supplementary Fig. S12). Further, we found that, after subtracting the baseline targeting of receivers without communication, each NR signalling module in a host tumour

was able to recruit more than 150 FXIII–NWs or more than 35,000 doxorubicin molecules encapsulated within FXIII–LPs (Supplementary Fig. S12), demonstrating the capacity for signal amplification in our approach. Similarly, each tTF–RGD signalling module that accumulated in a host tumour was able to recruit more than ten FXIII–NWs through induction of localized coagulation (Supplementary Fig. S12). The ability for each tumour-receptor-targeted tTF–RGD signalling module in our system to recruit many NP receiving modules contrasts to conventional strategies for ligand-mediated NP targeting, where, depending on NP valency, one or fewer NPs are delivered per ligand-bound receptor in tumours.

We believe that this work motivates a paradigm of 'systems nanotechnology' directed toward the construction of communicative diagnostic and therapeutic agents with sophisticated *in vivo* behaviours. Given the diverse NP and synthetic biological 'building blocks' under development[13–18,36–38], coupled with the plethora of robust biological cascades that could be re-purposed to enable communication between synthetic components, we believe that a wide array of nanosystems could be engineered to more sensitively locate, diagnose and treat a diversity of focal human diseases.

Methods

Signalling-module synthesis. Long-circulating PEG–NRs were synthesized with 5 kDa methoxy PEG–thiol coatings as described previously[23] and tTF–RGD and tTF–NGR signalling modules were expressed in engineered *Escherichia coli*, purified and tested *in vitro* to verify purity (>95%) and activity (factor-X coagulation test) as described in Supplementary Information.

Receiving-module synthesis. Peptide synthesis. The three peptides used in this work were synthesized through 9-fluorenyl-methoxycarbonyl solid-phase peptide synthesis, purified by high-performance liquid chromatography to >90% purity, and characterized through mass spectrometry as described in Supplementary Information.

Iron oxide NW synthesis. Superparamagnetic, dextran-caged iron oxide NWs with a longitudinal size of ~55 nm were synthesized, aminated using 20% v/v ammonium hydroxide, and derivatized with NIR fluorophores as described previously[11]. All peptide-functionalized NWs were characterized through dynamic light scattering and intravenously injected *in vivo* to ensure all targeted NWs and control NWs exhibited similar circulation times. NIR-fluorophore and peptide attachment protocols, along with NW purification methods, are provided in Supplementary Information.

Doxorubicin-loaded LP synthesis. Hydrogenated soy sn-glycero-3-phosphocholine (HSPC), cholesterol and 1,2-distearoyl-sn-glycero-3-phosphoethanolamine-*N*-polyethylene glycol 2000 (DSPE-PEG(2k)) and 1,2-distearoyl-sn-glycero-3-phosphoethanolamine-*N*-[maleimide(polyethylene glycol 2000)] (DSPE-PEG(2k)-MAL) were purchased from Avanti Polar Lipids. Doxorubicin was purchased from Sigma Chemical. Briefly, for targeted LP synthesis, LPs with maleimide groups were prepared from HSPC, cholesterol, DSPE-PEG(2k) and DSPE-PEG(2k)-MAL by lipid film hydration and membrane extrusion. Encapsulation of doxorubicin into the LPs was then carried out using a pH-gradient-driven loading protocol. Free doxorubicin was removed by gel filtration on Sephadex G-50 and the maleimide-terminated LPs were reacted with thiols on peptides (FXIII and FXIIIControl) for 2 h and then purified by gel filtration.

***In vivo* studies.** All studies in mice were approved by the Massachusetts Institute of Technology Committee on Animal Care. MDA-MB-435 human cancer cells were cultured as recommended by the American Type Culture Collection and injected into *nu/nu* mice to establish xenograft tumours as described previously[3,11,23].

Signalling-module distribution and bioactivity *in vivo*. Signalling-module biodistribution and fibrinogen coagulation assays are provided in Supplementary Information.

Immunohistochemical analysis in tumours. For histologic analysis, frozen sections of tumours were prepared. The sections were first fixed with acetone. Rat anti-mouse CD-31 (1:50, BD PharMingen) and biotinylated mouse fibrin(ogen) antiserum (1:50, Nordic) were used for immunochemical staining of tumour tissue sections. The corresponding secondary antibodies were added and incubated for 1 h at room temperature: AlexaFluor-594 goat anti-rat or rabbit IgG (1:1,000; Molecular Probes) and streptavidin Alexa Fluor 594 (1:1,000; Molecular Probes). The slides were washed three times with PBS and mounted in Vectashield Mounting Medium with 4,6-diamidino-2-phenylindole. At least three images from representative microscopic fields were analysed for each tumour sample.

Imaging receiving-NW homing to tumours. Mixtures of NIR-fluorophore-labelled, targeted and control NWs (bearing VT750 and VT680 or VT680 and VT750, respectively) were co-administered intravenously in PBS (2 mg Fe kg^{-1}) to tumour-bearing *nu/nu* mice to provide an internal control reference for coagulation-specific NW homing. At 24 h post NW injection, mice were killed and organs were analysed for both NIR fluorophores (LI-COR Odyssey Infrared Imaging System). For integrated NP-system characterization, mice were additionally imaged under isofluorane anaesthetic before killing using a whole-animal fluorescence reflectance imaging system (Xenogen, IVIS Imaging System) to visualize the specificity of NW homing to tumours. Images from both organ scanning and whole-animal imaging are displayed throughout the manuscript as overlaid green–red images from both fluorescence channels (VT750 = green and VT680 = red). For autonomously communicating nanosystems, NIR-fluorophore-labelled peptide-bearing NWs (bearing VT750 fluorophores) were intravenously (2 mg Fe kg^{-1}) in PBS to unanaesthetized MDA-MB-435 tumour-bearing *nu/nu* mice alone or alongside various tTF signalling modules (25 μg). At 24 h post NW injection, mice were killed and organs were analysed for NIR-receiver fluorescence (LI-COR Odyssey Infrared Imaging System). For intraoperative fluorescent tumour imaging, mice were anaesthesized and tumours were surgically exposed to reveal detailed tumour fluorescence (LI-COR). For whole-animal organ distribution, tTF–RGD signalling modules were administered intraperitoneally (25 μg) and FXIII–NWs were administered intravenously (2 mg Fe kg^{-1}) to mice bearing a single MDA-MB-435 tumour.

Quantification of receiver homing to tumours. Protocols for fluorescent quantification of NW and doxorubicin quantification are provided in Supplementary Information.

Therapeutic assessment of communicating and control NP systems. Therapeutic studies were conducted by first intravenously administering PEG–NRs or saline into *nu/nu* mice bearing a single MDA-MB-435 tumour. At 72 h post-injection, mice were intravenously administered FXIII–LPs, FXIIIControl–LPs or saline (in a ~150 μl bolus) and broadly irradiated in the vicinity of the tumour with NIR light (810 nm, ~1 W cm^{-2}, 20 min). An additional cohort of mice was administered saline at 0 and 72 h and not exposed to NIR light to isolate any therapeutic efficacy of this input in isolation. At regular intervals after treatment, tumours were measured and mice were weighed. Mice were killed when tumours exceeded 500 mm^3.

Received 15 November 2010; accepted 17 May 2011; published online 19 June 2011

References

1. Chan, W. C. & Nie, S. Quantum dot bioconjugates for ultrasensitive nonisotopic detection. *Science* **281,** 2016–2018 (1998).
2. Park, J. H. *et al.* Magnetic iron oxide nanoworms for tumour targeting and imaging. *Adv. Mater.* **20,** 1630–1630 (2008).
3. Xia, Y. N. & Halas, N. J. Shape-controlled synthesis and surface plasmonic properties of metallic nanostructures. *MRS Bull.* **30,** 338–344 (2005).
4. Gref, R. *et al.* Biodegradable long-circulating polymeric nanospheres. *Science* **263,** 1600–1603 (1994).
5. Sengupta, S. *et al.* Temporal targeting of tumour cells and neovasculature with a nanoscale delivery system. *Nature* **436,** 568–572 (2005).
6. Park, J. H., von Maltzahn, G., Ruoslahti, E., Bhatia, S. N. & Sailor, M. J. Micellar hybrid nanoparticles for simultaneous magnetofluorescent imaging and drug delivery. *Angew. Chem. Int. Ed.* **47,** 7284–7288 (2008).
7. Litzinger, D. C. & Huang, L. Phosphatidylethanolamine liposomes—drug delivery, gene-transfer and immunodiagnostic applications. *Biochim. Biophys. Acta* **1113,** 201–227 (1992).
8. Akinc, A. *et al.* A combinatorial library of lipid-like materials for delivery of RNAi therapeutics. *Nature Biotechnol.* **26,** 561–569 (2008).
9. Anderson, D. G., Lynn, D. M. & Langer, R. Semi-automated synthesis and screening of a large library of degradable cationic polymers for gene delivery. *Angew. Chem. Int. Ed.* **42,** 3153–3158 (2003).
10. Leserman, L. D., Barbet, J., Kourilsky, F. & Weinstein, J. N. Targeting to cells of fluorescent liposomes covalently coupled with monoclonal antibody or protein A. *Nature* **288,** 602–604 (1980).
11. Heath, T. D., Fraley, R. T. & Papahdjopoulos, D. Antibody targeting of liposomes: Cell specificity obtained by conjugation of F(ab′)2 to vesicle surface. *Science* **210,** 539–541 (1980).
12. Akerman, M. E., Chan, W. C. W., Laakkonen, P., Bhatia, S. N. & Ruoslahti, E. Nanocrystal targeting *in vivo*. *Proc. Natl Acad. Sci. USA* **99,** 12617–12621 (2002).
13. Hood, J. D. *et al.* Tumour regression by targeted gene delivery to the neovasculature. *Science* **296,** 2404–2407 (2002).
14. Farokhzad, O. C. *et al.* Nanoparticle–aptamer bioconjugates: A new approach for targeting prostate cancer cells. *Cancer Res.* **64,** 7668–7672 (2004).
15. Weissleder, R., Kelly, K., Sun, E. Y., Shtatland, T. & Josephson, L. Cell-specific targeting of nanoparticles by multivalent attachment of small molecules. *Nature Biotechnol.* **23,** 1418–1423 (2005).
16. Geng, Y. *et al.* Shape effects of filaments versus spherical particles in flow and drug delivery. *Nature Nanotech.* **2,** 249–255 (2007).
17. Moghimi, S. M., Hunter, A. C. & Murray, J. C. Long-circulating and target-specific nanoparticles: Theory to practice. *Pharmacol. Rev.* **53,** 283–318 (2001).

18. Moghimi, S. M. & Szebeni, J. Stealth liposomes and long circulating nanoparticles: Critical issues in pharmacokinetics, opsonization and protein-binding properties. *Progr. Lipid Res.* **42,** 463–478 (2003).
19. Murphy, C. J. *et al.* Anisotropic metal nanoparticles: Synthesis, assembly, and optical applications. *J. Phys. Chem. B* **109,** 13857–13870 (2005).
20. Jain, P. K., Lee, K. S., El-Sayed, I. H. & El-Sayed, M. A. Calculated absorption and scattering properties of gold nanoparticles of different size, shape, and composition: Applications in biological imaging and biomedicine. *J. Phys. Chem. B* **110,** 7238–7248 (2006).
21. Hu, M. *et al.* Gold nanostructures: Engineering their plasmonic properties for biomedical applications. *Chem. Soc. Rev.* **35,** 1084–1094 (2006).
22. Kong, G., Braun, R. D. & Dewhirst, M. W. Hyperthermia enables tumour-specific nanoparticle delivery: Effect of particle size. *Cancer Res.* **60,** 4440–4445 (2000).
23. von Maltzahn, G. *et al.* Computationally-guided photothermal tumour therapy using long-circulating gold nanorod antennas. *Cancer Res.* **69,** 3892–3900 (2009).
24. Hashizume, H. *et al.* Openings between defective endothelial cells explain tumour vessel leakiness. *Am. J. Pathol.* **156,** 1363–1380 (2000).
25. Maeda, H. The enhanced permeability and retention (EPR) effect in tumour vasculature: The key role of tumour-selective macromolecular drug targeting. *Adv. Enzyme Regul.* **41,** 189–207 (2001).
26. Weissleder, R. A clearer vision for *in vivo* imaging. *Nature Biotechnol.* **19,** 316–317 (2001).
27. Kessler, T. *et al.* Inhibition of tumour growth by RGD peptide-directed delivery of truncated tissue factor to the tumour vasculature. *Clin. Cancer Res.* **11,** 6317–6324 (2005).
28. Bieker, R. *et al.* Infarction of tumour vessels by NGR-peptide directed targeting of tissue factor. Experimental results and first-in-man experience. *Blood* **113,** 5019–5027 (2009).
29. Huang, X. M. *et al.* Tumour infarction in mice by antibody-directed targeting of tissue factor to tumour vasculature. *Science* **275,** 547–550 (1997).
30. El-Sheikh, A., Borgstrom, P., Bhattacharjee, G., Belting, M. & Edgington, T. S. A selective tumour microvasculature thrombogen that targets a novel receptor complex in the tumour angiogenic microenvironment. *Cancer Res.* **65,** 11109–11117 (2005).
31. Persigehl, T. *et al.* Antiangiogenic tumour treatment: Early noninvasive monitoring with USPIO-enhanced MR imaging in mice. *Radiology* **244,** 449–456 (2007).
32. Paborsky, L. R., Caras, I. W., Fisher, K. L. & Gorman, C. M. Lipid association, but not the transmembrane domain, is required for tissue factor activity. Substitution of the transmembrane domain with a phosphatidylinositol anchor. *J. Biol. Chem.* **266,** 21911–21916 (1991).
33. Jaffer, F. A. *et al.* Molecular imaging of factor XIIIa activity in thrombosis using a novel, near-infrared fluorescent contrast agent that covalently links to thrombi. *Circulation* **110,** 170–176 (2004).
34. Tung, C. H. *et al.* Novel factor XIII probes for blood coagulation imaging. *Chembiochem* **4,** 897–899 (2003).
35. Overoye-Chan, K. *et al.* EP-2104R: A fibrin-specific gadolinium-based MRI contrast agent for detection of thrombus. *J. Am. Chem. Soc.* **130,** 6025–6039 (2008).
36. Isaacs, F. J., Dwyer, D. J. & Collins, J. J. RNA synthetic biology. *Nature Biotechnol.* **24,** 545–554 (2006).
37. Hasty, J., McMillen, D. & Collins, J. J. Engineered gene circuits. *Nature* **420,** 224–230 (2002).
38. Jungmann, R., Renner, S. & Simmel, F. C. From DNA nanotechnology to synthetic biology. *HFSP J.* **2,** 99–109 (2008).

Acknowledgements

This work was supported by the National Cancer Institute of the National Institutes of Health through grant numbers U54 CA 119335 (UCSD CCNE), 5-R01-CA124427 (Bioengineering Research Partnerships, BRP), U54 CA119349 (MIT CCNE) and 5 P30 CA30199-28 (SBMRI Cancer Center Support Grant). Work in the Muenster laboratory is supported by Deutsche Forschungsgemeinschaft (SFB 656/C8 Mesters) and German Cancer Aid (109245 Berdel). G.v.M. acknowledges support from Whitaker and NSF Graduate Fellowship. The authors thank P. Caravan for assistance with the fibrin-binding peptide selection and testing, D. Kim, S. Mo, L. Ong and M. Xu for assistance with *in vivo* studies and R. Weissleder for assistance with preliminary fluorescent imaging studies.

Author contributions

G.v.M. and S.N.B. conceived the communication strategy, analysed results and wrote the manuscript; G.v.M., J-H.P., K.Y.L. and N.S. designed and carried out experiments; C.S., R.M., W.E.B., E.R. and M.J.S. contributed reagents and technical expertise.

Additional information

The authors declare no competing financial interests. Supplementary information accompanies this paper on www.nature.com/naturematerials. Reprints and permissions information is available online at http://www.nature.com/reprints. Correspondence and requests for materials should be addressed to S.N.B.